J. Fluid Mech. (1982), *vol.* 115, *pp.* 105–121
Printed in Great Britain

Vortex-flow regimes

By M. P. ESCUDIER AND N. ZEHNDER
Brown Boveri Research Centre, 5405 Baden-Dättwil, Switzerland

(Received 30 March 1981)

Analysis of a considerable body of new data, based upon flow-visualization experiments, reveals a simple criterion for the occurrence of vortex breakdown at a fixed location in a tube: $Re_B \sim \Omega^{-3} R^{-1}$, where Ω is the circulation number, R the ratio of the radial to tangential velocities in the inflow region, and Re_B the pipe Reynolds number at which vortex breakdown occurs. The constant of proportionality is found to be practically independent both of the pipe flare angle α and the type of breakdown observed (bubble, spiral, etc.) although the latter is shown to depend on Re_B. Theoretical support for the experimental results is derived from the analysis of Benjamin (1962) combined with similarity arguments.

1. Introduction

The two predominant forms of vortex breakdown, the (axisymmetric) bubble and (non-axisymmetric) spiral, were first identified in the leading-edge vortices generated by flow over delta wings at incidence and their qualitative features clearly described by Lambourne & Bryer (1961). Subsequent experiments on vortex breakdown, performed for the more controlled situation of flow in cylindrical or flared tubes with swirl introduced by upstream guide vanes, have been reported by Harvey (1962), Kirkpatrick (1964), Lambourne (1965), Cassidy & Falvey (1970), Sarpkaya (1971*a*, *b*, 1974), Ikeda, Sakata & Kikuchi (1974), Bellamy-Knights (1976), Faler & Leibovich (1977, 1978), and Garg & Leibovich (1979). Sarpkaya (1971*a*) identified a third form of breakdown, the double helix, and Faler & Leibovich (1977) describe a total of six distinct modes of disruption of a vortex core (including vortex breakdown) as the Reynolds number and circulation number are varied. Much of what is now known about vortex disruption is based upon flow visualization and is therefore largely descriptive and inevitably to some extent subjective, although Leibovich and his co-workers as well as the present authors and their co-workers (Escudier *et al.* 1980*a*, *b*) have recently reported some detailed measurements of vortex flowfields performed using laser–Doppler anemometers (LDA).

It is generally accepted that vortex flows may be classified as either supercritical or subcritical, with vortex breakdown representing the transition from one flow regime to the other. However, in spite of the considerable effort which has been expended on the investigation of vortex flows, until now there has been no general framework to guide the choice of values for the controlling parameters and within which to discuss observations of breakdown and other vortex phenomena and in particular no criteria by which to specify whether a vortex flow would be subcritical

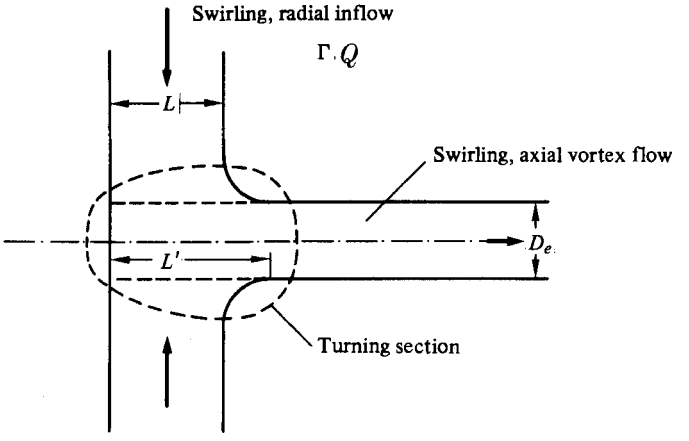

FIGURE 1. Arrangement of hypothetical vortex experiment.

or supercritical. The basis for such a framework was proposed recently by Escudier *et al.* (1980*b*), and the present work represents a generalization of their classification scheme. To some extent progress has been hindered by the lack of reliable theoretical description of vortex behaviour. Indeed it seems to be the case that the appealing theoretical simplification of *local* quasi-cylindricity has caused previous investigators to overlook the fact that non-cylindrical influences *upstream* must affect the radial structure of the vortex and that such influences should at least remain unchanged as other parameters are varied. To illustrate this point we consider the hypothetical vortex experiment depicted in figure 1. Fluid of kinematic viscosity ν flows into the system, which is axisymmetric, with uniform circulation Γ and volume flow rate Q uniformly distributed along the inlet length L. In the section indicated by the broken curve, the flow is turned into the axial direction and passes through the tube of diameter D_e where the vortex flow is to be observed. From dimensional considerations, it is apparent that a complete description of the vortex flow for a given geometry must include at least the three dynamic parameters

$$Q/D_e\nu, \quad \Gamma D_e/Q, \quad Q/\Gamma L, \tag{1}$$

or their equivalent. For consistency with previous investigators we introduce the mean axial velocity in the vortex tube $w_e \equiv 4Q/\pi D_e^2$, a radial velocity $U \equiv Q/\pi DL$ and a swirl velocity $V \equiv \Gamma/\pi D$. We can then redefine our three parameters as

$$Re \equiv w_e D_e/\nu, \quad \Omega \equiv \Gamma/w_e D_e, \quad R \equiv U/V, \tag{2}$$

the first two of which are the usual Reynolds number and circulation number, whilst R is just the ratio of the radial velocity to the tangential velocity in the inflow section, i.e. the cotangent of the inflow angle. It is the independent role of the latter parameter which has not received mention in the past, probably because in the most commonly employed experimental setup (essentially that described in some detail by Sarpkaya (1971*a*) although a similar system, later used by Harvey (1962), was described earlier by Titchener & Taylor-Russell (1956)), as swirl vanes are adjusted to increase Ω, ΩR remains constant ($= \pi D_e/(4L)$) and so the separate influences of Ω and R cannot be inferred.

In the present paper we present the results of an extensive series of observations

of vortex disturbances (primarily breakdown) in an experimental arrangement in which Ω, R and Re can be varied independently. The results confirm the independent significance of R and suggest that over a wide range of conditions a simple power-law relationship exists between the Reynolds number at which vortex breakdown occurs, Re_B, and Ω, i.e. $Re_B \sim \Omega^{-3}$. Theoretical considerations, show that for consistency R should enter the relationship as R^{-1}, i.e. $Re_B \sim \Omega^{-3}R^{-1}$, and this too is largely confirmed by the experimental results.

2. Experimental apparatus

The experimental set-up, shown schematically in figure 2, is similar to that employed by Escudier *et al.* (1980*a*) but with minor modifications to permit coverage of as wide a range of the flow parameters as possible. The Plexiglas vortex tube, which forms part of a gravity-fed water circuit, has an internal diameter $D = 55$ mm and an overall length $L = 486$ mm. The flow enters the generator section of the tube through a tangential inlet slit, the width t of which can be varied through the use of inserts. The observations of vortex breakdown and other disturbed vortex states are made in contraction sections which have a length of 83 mm and can be installed in the 55 mm tube at various axial locations L. Whilst the earlier work of the present authors and their co-workers was primarily concerned with the flow in the generator section, the present paper concentrates on the flow in the contraction which plays a key role in determining the nature of the vortex core in the upstream region. Results are reported here for cylindrical contractions of diameter D_e as well as for flared contractions of inlet diameter D_e and total divergence angle α. The inlet slit is blocked downstream of the generator section, as shown in figure 2, to minimize any axial flow in the inlet. A careful check was maintained on the water temperature, which varied during the course of the experiments between about 8 and 20 °C with a corresponding change in kinematic viscosity from $1{\cdot}38 \times 10^{-6}$ to $1{\cdot}00 \times 10^{-6}$ m^2 s^{-1}. For flow visualization, water-soluble dyes were injected into the flow through two 1 mm-diameter holes in the tube end wall, one located on the axis and the other displaced radially by 18 mm. For the camera set-up employed, radial distances appear about 25 % larger than reality owing to refraction at the outer surface of the tube.

Based upon the swirl-velocity measurements reported recently for flow in our system (Escudier *et al.* 1980*a*), the circulation is assumed to be given by $\Gamma = \pi DV$, where $V \equiv Q/tL$ is the mean velocity in the inlet slit. An equivalent radial velocity U is defined by averaging the inflow Q over a length L of the surface of the 55 mm tube, i.e. $U = Q/(\pi DL)$. The three non-dimensional parameters may then be evaluated for our experimental set-up as follows:

$$\left.\begin{array}{ll} \text{Reynolds number} & Re \equiv w_e D_e/\nu = 4Q/\pi D_e \nu; \\ \text{circulation number} & \Omega \equiv \Gamma/w_e D_e \simeq \pi^2 DD_e/4Lt; \\ \text{velocity ratio} & R \equiv Q/\Gamma L \simeq t/\pi D. \end{array}\right\} \tag{3}$$

At this point an important feature of our arrangement becomes apparent: both Ω and Re can be varied independently whilst maintaining R constant. This advantage over the more usual swirl-vane arrangement more than offsets the disadvantage that

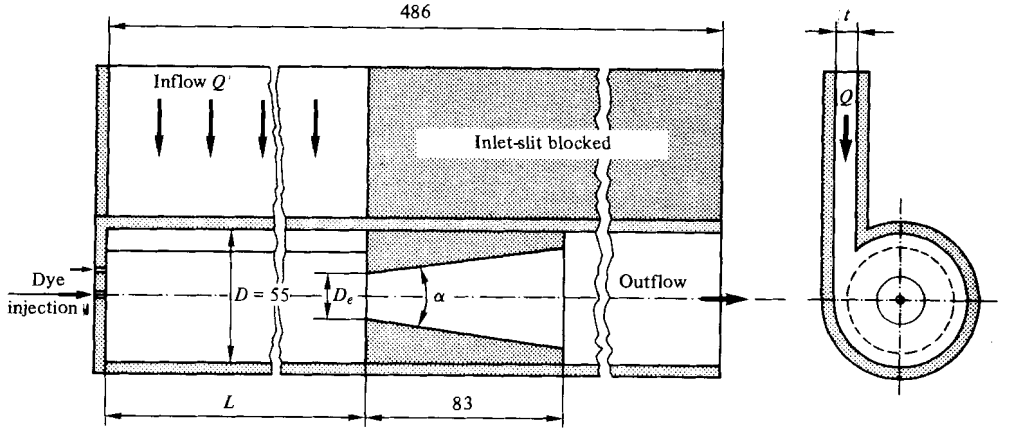

FIGURE 2. Schematic diagram of the vortex tube (linear dimensions in mm).

L(mm)	58·5, 108·5, 158·5, 208·5, 258·5, 308·5, 358·5
t(mm)	2, 4, 6, 8, 10
D_e(mm)	10, 12, 15, 18, 21, 25, 32, 40, 47, 55
$\alpha(^\circ)$	3, 5, 10, 15, 20, 25
$Q(\mathrm{m^3\,s^{-1}})$	3×10^{-6}–$1{\cdot}4\times10^{-3}$
Re	$0{\cdot}80\times10^{2}$–$1{\cdot}04\times10^{5}$
Ω	0·66–46·4
R	0·012–0·058

TABLE 1. Ranges of values for physical and non-dimensional parameters investigated.

a single tangential inlet slit inevitably introduces a lack of axisymmetry into the flow. It may also be noted that the value of Ω depends upon three quantities which can be varied independently: D_e, L and t. However, not all possible combinations of the geometrical parameters were investigated, the number of experiments with flared contractions in particular being rather limited. The range of values covered by both the physical and non-dimensional parameters are listed in table 1.

3. Observations

Figure 3 is constituted from a representative series of photographs of the flow states, primarily vortex breakdown, observable in cylindrical contractions for a generator tube with $t = 8$ mm ($R = 0{\cdot}046$) as Re is varied for a series of decreasing values of the parameter Ω. With minor variations, similar photographs could be given for the other possible slit widths, though with different values for Ω (see §4). Figure 4 is made up of a similar series of photographs for flared contractions.

Since detailed descriptions of such photographs have been given by Sarpkaya (1971*a*, *b*) and Faler & Leibovich (1977), we shall keep our remarks as brief as possible and emphasize those characteristics which have special significance.

For a parallel contraction with flow at a low Reynolds number and high circulation number, the vortex core is laminar throughout the generator tube and contraction and becomes noticeably unstable only downstream of the contraction. A sufficient

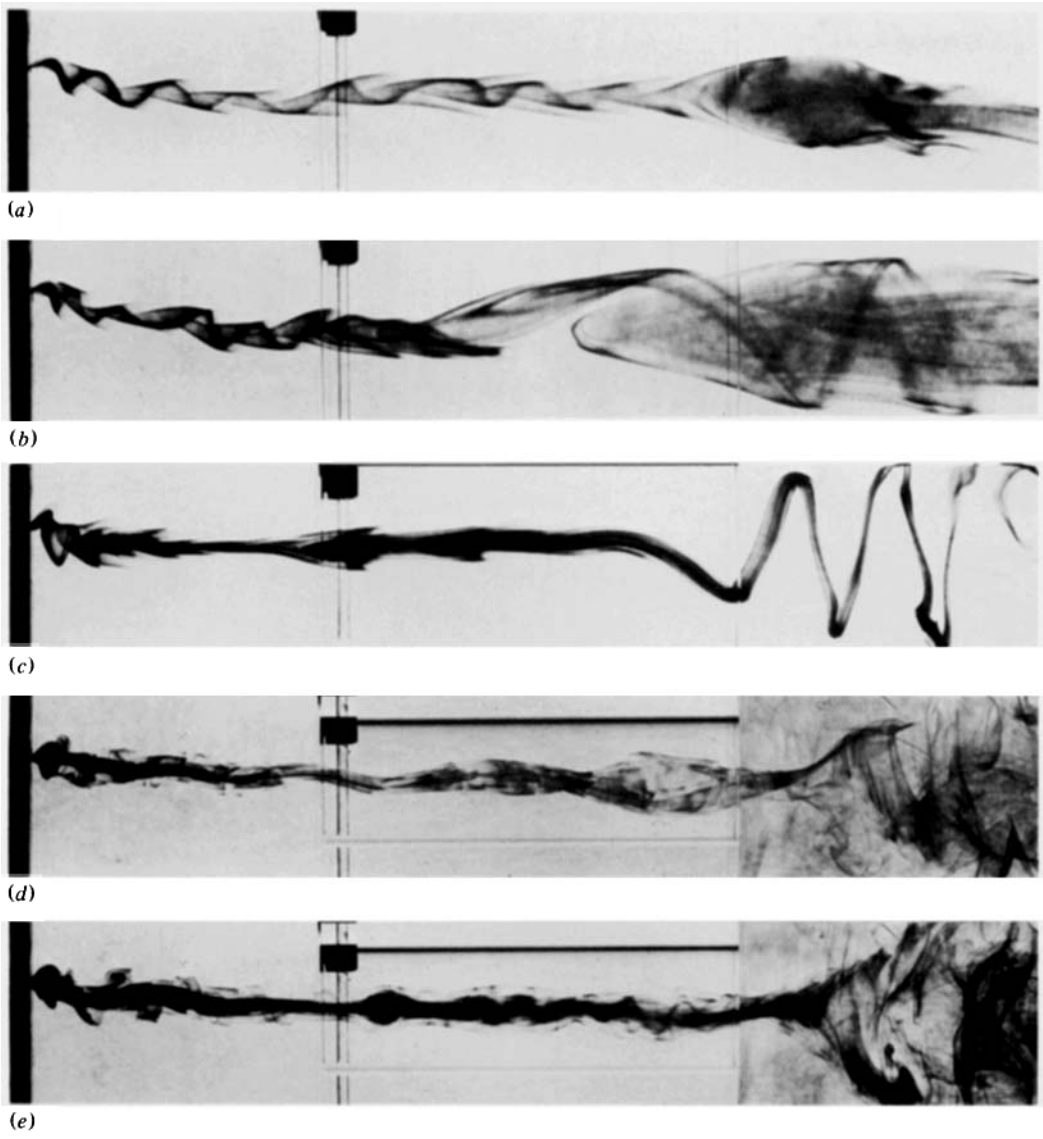

FIGURE 3(*a–e*). See p. 110.

slight increase in flowrate to give $Re = 140$ (for $\Omega = 11{\cdot}6$) produces a large bubble-like disturbance with its nose just inside the contraction and followed by a cylindrical, laminar wake (figure 3*a*). With a further slight increase in flow rate, to $Re = 180$, the bubble penetrates further upstream ultimately transforming into a spiral breakdown with a definite stagnation point close to the contraction inlet (figure 3*b*). Further increases in flow rate result first in a smeared out spiral structure occupying the whole contraction and ultimately in a turbulent core with no distinct structure extending all the way upstream to the end wall. In direct contrast to the observations of Sarpkaya and of Leibovich and his co-workers, the sense of these spirals in our experiments is unmistakably opposite to that of the swirling flow within which they

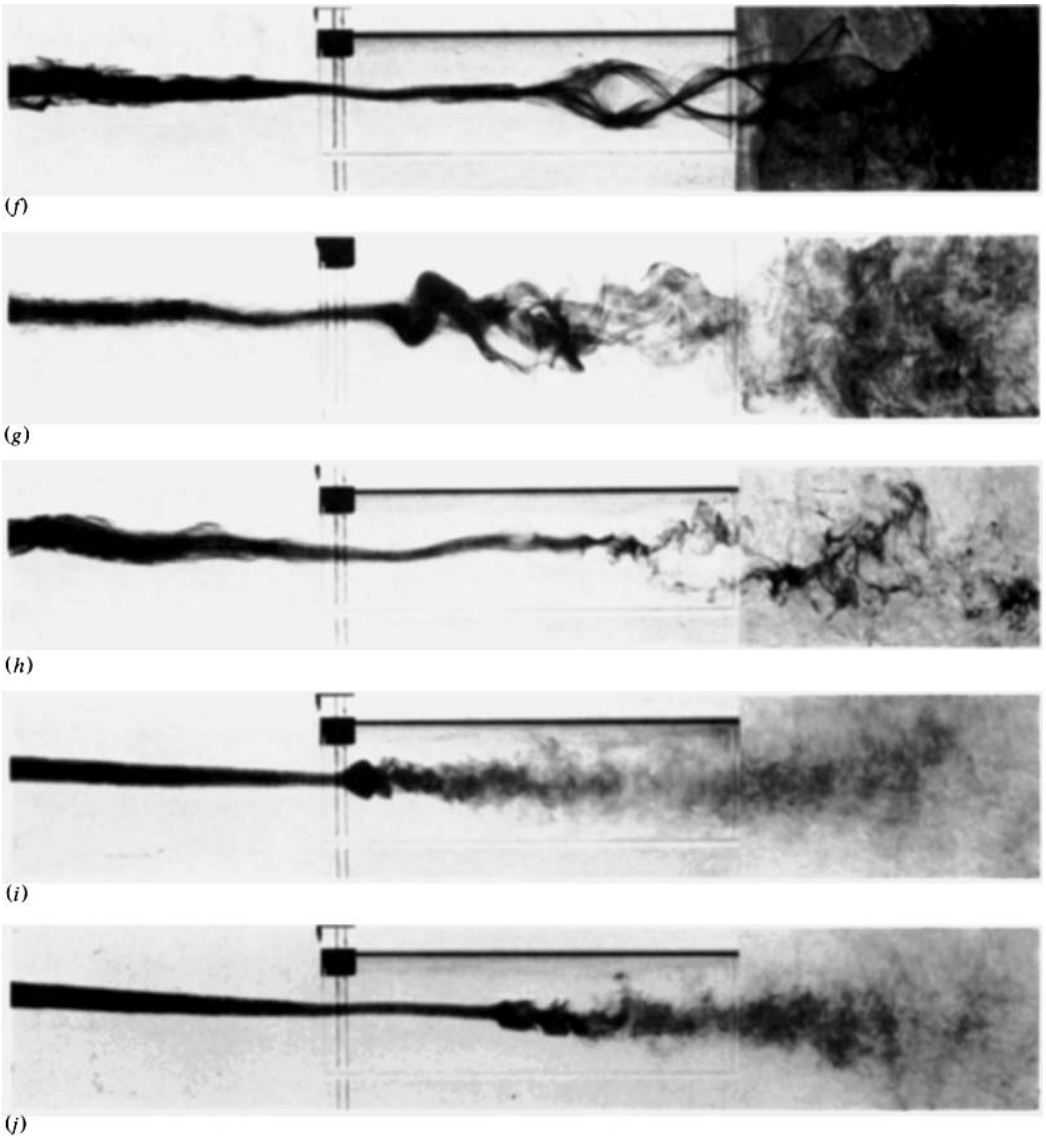

FIGURE 3. Photographs of vortex-breakdown forms and prebreakdown disturbances in cylindrical contractions. (*a*) $\Omega = 11{\cdot}60$, $Re = 140$; (*b*) $\Omega = 11{\cdot}60$, $Re = 180$; (*c*) $\Omega = 9{\cdot}28$, $Re = 270$; (*d*) $\Omega = 5{\cdot}22$, $Re = 550$; (*e*) $\Omega = 5{\cdot}22$, $Re = 660$; (*f*) $\Omega = 2{\cdot}81$, $Re = 1350$; (*g*) $\Omega = 2{\cdot}60$, $Re = 2900$; (*h*) $\Omega = 1{\cdot}46$, $Re = 3300$; (*i*) $\Omega = 1{\cdot}46$, $Re = 15000$; (*j*) $\Omega = 1{\cdot}46$, $Re = 15000$.

are embedded. Lambourne & Bryer (1961) also observed that for their leading-edge vortices the sense of the spiral was opposite to that of the vortex itself.

If the circulation number is reduced, a large bubble again appears at the contraction exit at a fairly low Reynolds number ($Re = 200$ for $\Omega = 9{\cdot}28$). However, with an increase in flow rate (to $Re = 270$) the large bubble is replaced by a small bubble-like swelling located near the contraction inlet ($\simeq 10$ mm downstream) and followed by a well-defined large-scale spiral at the exit (figure 3*c*). A similar sequence of events is observed for lower circulation numbers (down to about $\Omega = 6$), and

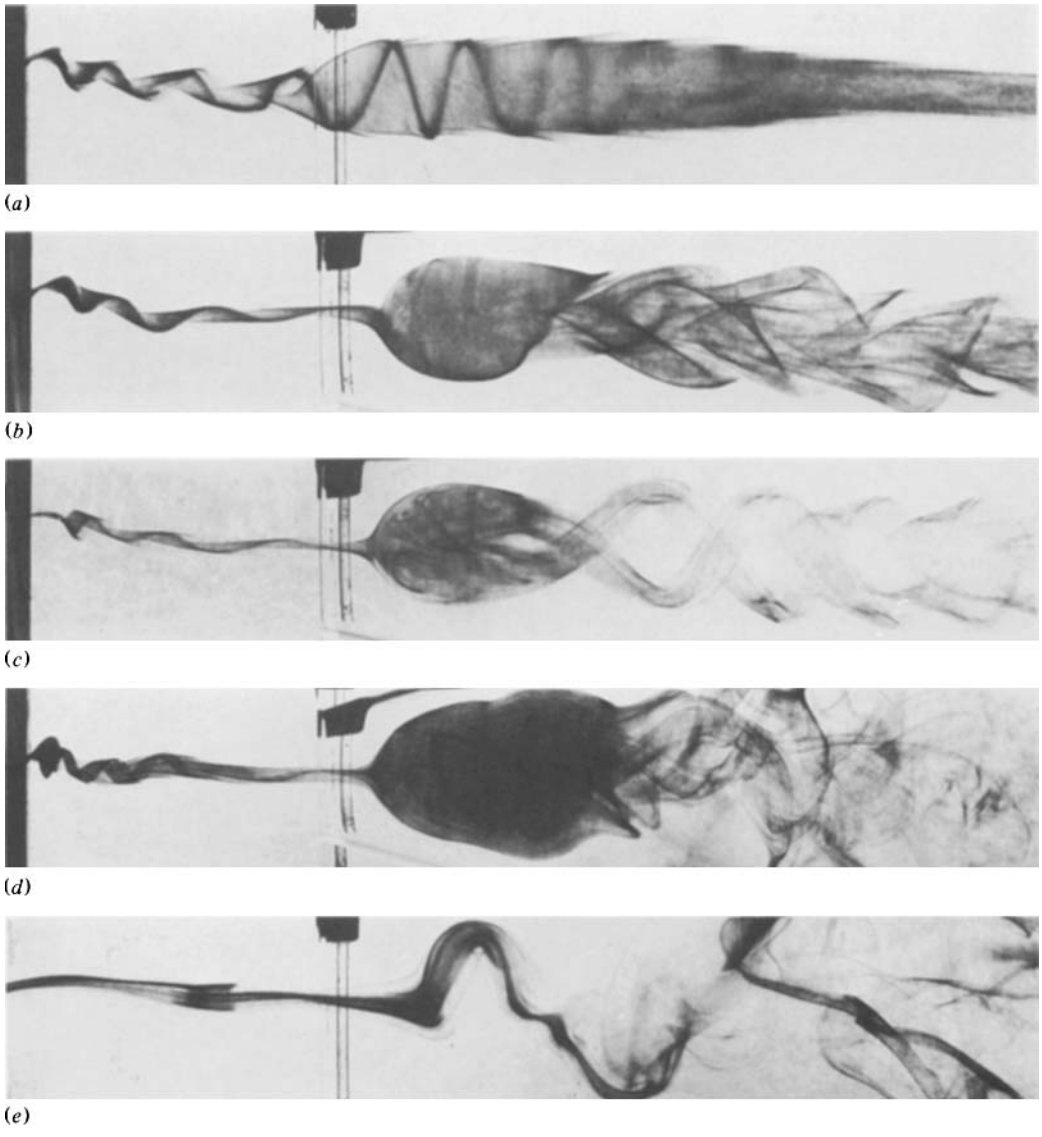

FIGURE 4(*a–e*). See p. 112.

correspondingly higher Reynolds numbers, though the exit bubble and spiral become less distinct and the flow takes on an increasingly turbulent character.

For circulation numbers with values below about six, the vortex becomes noticeably disturbed at lower Reynolds numbers than those corresponding to vortex breakdown. An example of this 'prebreakdown disturbance' is given in figure 3(*d*) for $\Omega = 5{\cdot}22$ and $Re = 550$. The core is turbulent in the generator tube (though with fluctuations in the radial direction clearly suppressed owing to the swirl) but relaminarizes (or at least becomes much less turbulent) as it accelerates into the contraction. Sporadically, about halfway along the contraction, the core spreads out into a meandering and spiralling ribbon. This ribbon structure, for the larger Reynolds numbers, always precedes the appearance of vortex breakdown and may

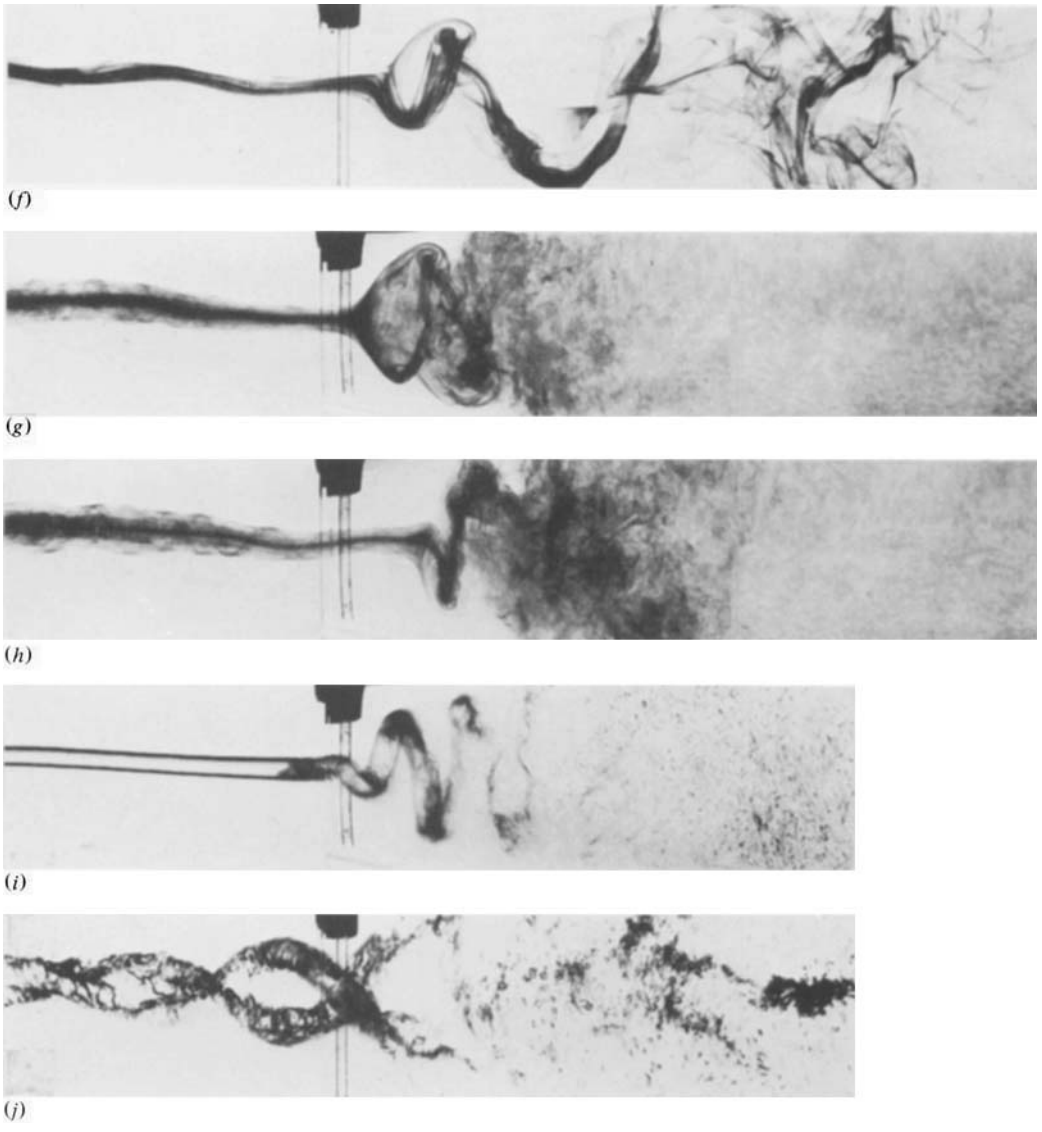

FIGURE 4. Photographs of vortex breakdown forms in flared contractions. (*a*) $\Omega = 11{\cdot}60$, $\alpha = 10°$, $Re = 130$; (*b*) $\Omega = 7{\cdot}25$, $\alpha = 20°$, $Re = 220$; (*c*) $\Omega = 7{\cdot}25$, $\alpha = 20°$, $Re = 220$; (*d*) $\Omega = 5{\cdot}22$, $\alpha = 25°$, $Re = 400$; (*e*) $\Omega = 4{\cdot}28$, $\alpha = 10°$, $Re = 510$; (*f*) $\Omega = 3{\cdot}25$, $\alpha = 10°$, $Re = 1100$; (*g*) $\Omega = 2{\cdot}03$, $\alpha = 20°$, $Re = 3800$; (*h*) $\Omega = 2{\cdot}03$, $\alpha = 20°$, $Re = 3800$; (*i*) $\Omega = 1{\cdot}37$, $\alpha = 20°$, $Re = 160000$; (*j*) $\Omega = 3{\cdot}25$, $\alpha = 10°$, $Re = 90000$.

well represent a laminar/turbulent transition. With an increase in Reynolds number, Ω remaining unchanged, a bubble-type disturbance appears just ahead of the ribbon (i.e. about halfway along the contraction). Such a bubble is not stable, but may both fluctuate in longitudinal position and also disappear and reappear randomly. At a sufficiently high flow rate, however, the breakdown moves upstream to about 10 mm from the contraction inlet and is followed by a spiralling wake, the sense of the spiral being again opposite to that of the external flow (figure 3*e*). For Ω between 4·5 and 2·0, and Re between 600 and 2000, respectively, the prebreakdown disturbance takes

the form of a ribbon split into two or more strands, as seen in figure 3(*f*). Here, as in figure 3(*d*), the sense of the spiral is the same as that of the outer flow. The corresponding breakdown, as in figure 3(*g*), contains elements of both the spiral and bubble forms, again with an opposite-sense spiral wake. The sequence just described persists as the circulation number is decreased, with the spiralling ribbon first appearing at ever higher Reynolds numbers with an increasingly complex structure (figure 3*h*) and increasingly separated from the bubble/spiral breakdown. The breakdown structure also becomes less distinct, although the bubble and spiral forms are still identifiable and may alternate with each other, the former always appearing upstream of the latter, as in figures 3(*i*) and 3(*j*). A limiting factor for the smaller diameter contractions is the onset of cavitation at high flow rates.

For strongly flared contractions, a somewhat similar sequence of events is observed with the important difference that the scale of the vortex breakdown is considerably increased and the structure much better defined. Also there was no clearly evident prebreakdown disturbance. Typical examples of the various breakdown forms observed in flared contractions are shown in figure 4. With $\Omega = 7{\cdot}25$, two types of breakdown could be obtained at the same Reynolds number, $Re = 220$ (figures 4*b*,*c*), both of which were quite stable. Whether the single- or the double-tailed version would be obtained was entirely unpredictable. Two different forms, the bubble (figure 4*g*) and the spiral (figure 4*h*), were also obtained for $\Omega = 2{\cdot}03$, $Re = 3800$, though in this case the two alternated spontaneously, much as for the cylindrical contraction with $\Omega = 1{\cdot}46$.

The final two photographs in the series (figures 4*i*, *j*) are for cavitating flows, the first having the same form as a spiral breakdown (which occurs at a much lower flow rate, figure 4*h*) and the second the form of a double spiral. These two photographs are included because in contrast to the dye photographs the opposite sense of the spiral is clearly apparent owing to the shadows cast (viewed from downstream, the sense of rotation of the outer flow is clockwise).

A general observation for both cylindrical and flared contractions is that vortex breakdown becomes increasingly steady as the circulation number is increased.

4. Measurements

For each of the five inlet slit widths ($t = 2$, 4, 6, 8, 10 mm) a series of experiments was carried out to determine the Reynolds number Re_P at which the prebreakdown disturbance was first observed in a cylindrical contraction and the Reynolds number Re_B at which a clearly defined breakdown occurred just downstream ($\simeq 10$ mm) of the contraction inlet. At this location, the breakdown structure is well defined and relatively stable, and wall-friction influences are likely to be relatively insignificant. With a decrease in flow rate, the breakdown could always be moved to a location further downstream. However, once the breakdown reached the midpoint of the contraction, it either disappeared or jumped beyond the contraction outlet. A few measurements relating to this behaviour have been reported by Escudier *et al.* (1980*b*). For each slit width (i.e. value of the velocity-ratio parameter R), the circulation number Ω was varied over as wide a range as possible by changing the contraction diameter D_e and the contraction position L. The results are plotted on double-logarithmic scales in figures 5–8.

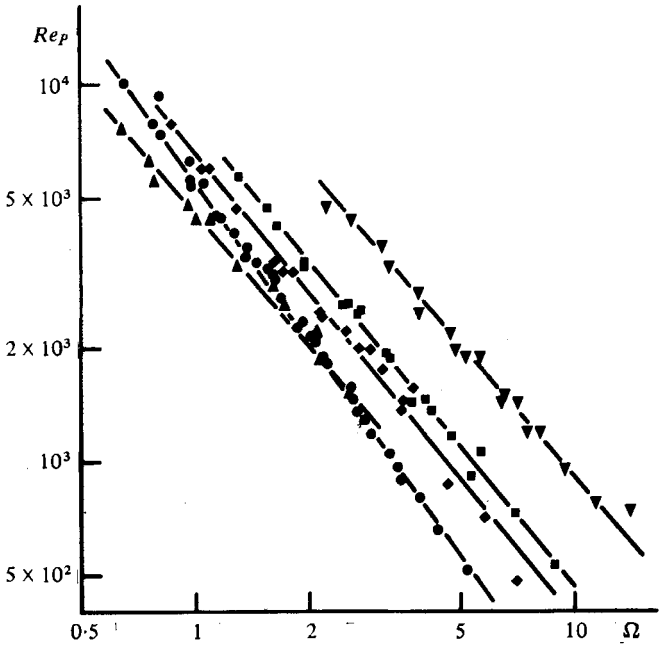

FIGURE 5. Prebreakdown-disturbance data for cylindrical contractions. Values of R: ▼, 0·012; ■, 0·023; ◆, 0·035; ●, 0·046; ▲, 0·058.

The prebreakdown data (figure 5) lie on a series of near-parallel straight lines with slope $\simeq -\frac{4}{3}$. The breakdown data for the longer inlet slits ($L > 108{\cdot}5$ mm) (figure 6) follow a similar trend, but with slope $\simeq -3$. Both sets of data confirm that the inclusion of R as an independent parameter is essential in any general representation of breakdown data. The data for the two shorter inlet slits ($L = 58{\cdot}5$ and 108·5 mm, i.e. $L/D = 1{\cdot}06$ and 1·97, respectively) deviate from the systematic trends of the bulk of the breakdown data in two ways and have therefore been plotted separately in figure 7 with broken lines representing the data for $L/D > 2$. At low Reynolds numbers the points no longer follow a simple power-law relationship, and for $Re_B < 1000$ it was no longer possible to distinguish a prebreakdown disturbance. A more serious problem, however, is the departure of the data from a single curve for each value of R, especially as R is decreased: i.e. a dependence on L/D is observed. A possible explanation for this behaviour is that in such short tubes the flow (particularly the core size) does not satisfy the conditions required for dynamical similarity (see below). In addition, it is probable that there are influences associated with the close proximity of the end wall and the contraction inlet.

It is convenient at this point to introduce some theoretical considerations† based upon the work of Benjamin (1962) and the concepts of similarity. If as scaling quantities we introduce L, Γ, w_e and the core radius r_c into the cylindrical axisymmetric form of the Navier–Stokes equations for a low-viscosity, incompressible, Newtonian fluid, it can be shown that for small cores ($r_c/L \ll 1$) two independent parameters are required to describe the core flow

$$\frac{\nu L}{w_e r_c^2} \quad \text{and} \quad \frac{\Gamma}{2\pi r_c w_e}.$$

† The authors are indebted to Dr J. J. Keller for the discussion given here.

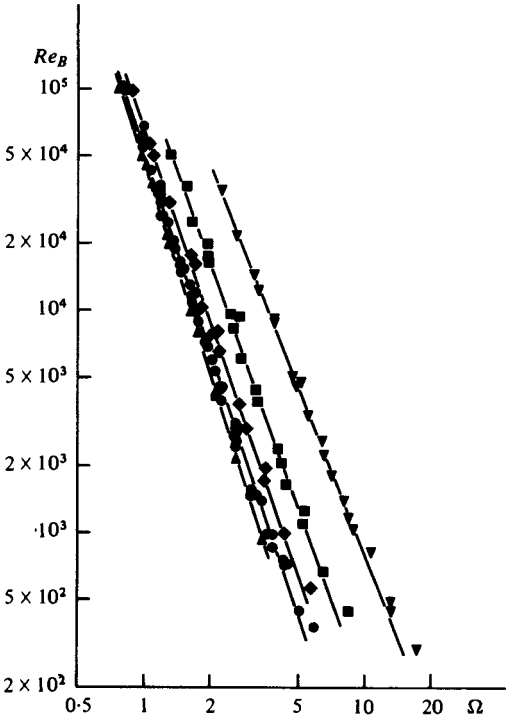

FIGURE 6. Vortex-breakdown data for cylindrical contractions: long inlet slits ($L/D > 2$). For an explanation of the symbols see figure 5.

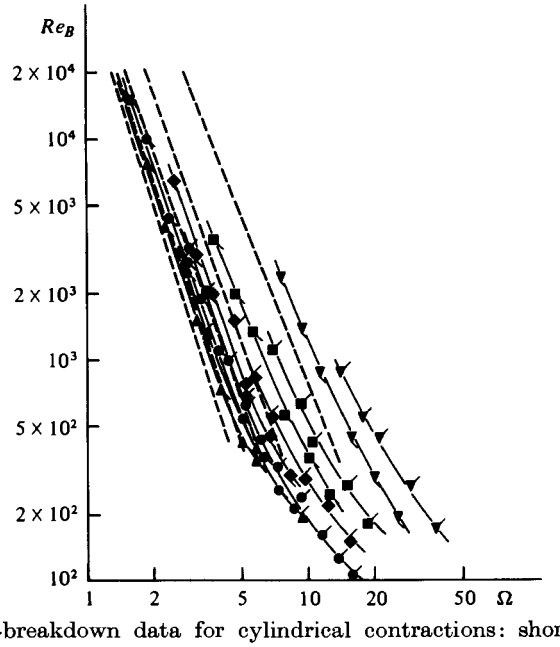

FIGURE 7. Vortex-breakdown data for cylindrical contractions: short inlet slits ($L/D < 2$). For an explanation of the symbols see figure 5. The upward tags are for $L/D = 1{\cdot}06$; the downward tags, $L/D = 1{\cdot}97$.

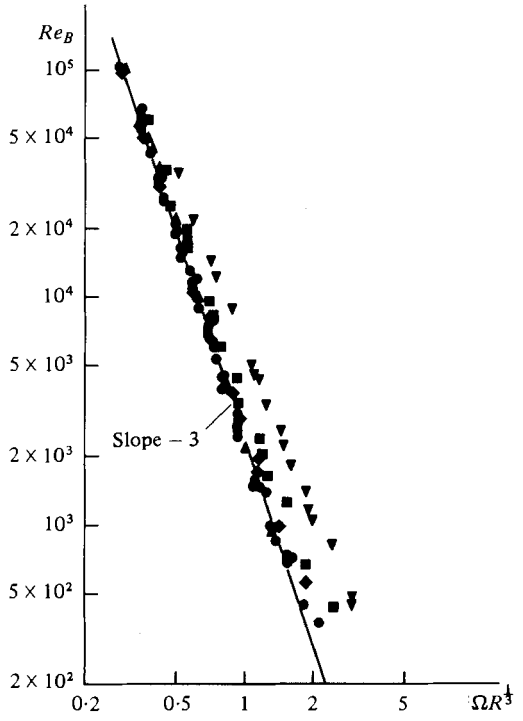

FIGURE 8. Vortex-breakdown data for cylindrical contractions: long inlet slits ($L/D > 2$). For an explanation of the symbols see figure 5.

It may also be shown that strict dynamical similarity, in which the inner viscous core (with now $r_c/r_e \ll 1$ in addition) is matched to an outer irrotational flow, requires that the first of these two parameters be invariant if the second is itself invariant within geometrically similar sets of geometries. From Benjamin's (1962) analysis it can be shown that a small vortex core ($r_c/r_e \ll 1$) becomes critical, the condition for mild vortex breakdown, for a particular value of the second parameter, provided the normalized velocity components remain invariant. Taken together, the preceding statements lead to the conclusion that the restriction to geometrically similar flow devices is compatible with the invariance of the first parameter and so justifies the use of

$$(\nu L/w_e)^{\frac{1}{2}},$$

as an invariant definition for the core radius r_c. It may be noted that this expression is identical with that given by similarity solutions such as have been discussed by Donaldson & Sullivan (1960).

Substitution of this result into the criticality criterion

$$\Gamma/(2\pi r_c w_e) = \text{constant},$$

then leads to

$$\Omega^3 R Re_B = \text{constant},$$

as a global criterion for vortex breakdown, it being understood that the constant is determined by the particular geometry.

To test the validity of the above result, the data of figure 6 have been replotted in figure 8 as Re_B versus $\Omega R^{\frac{1}{2}}$ (double-logarithmic co-ordinates). The collapse of the

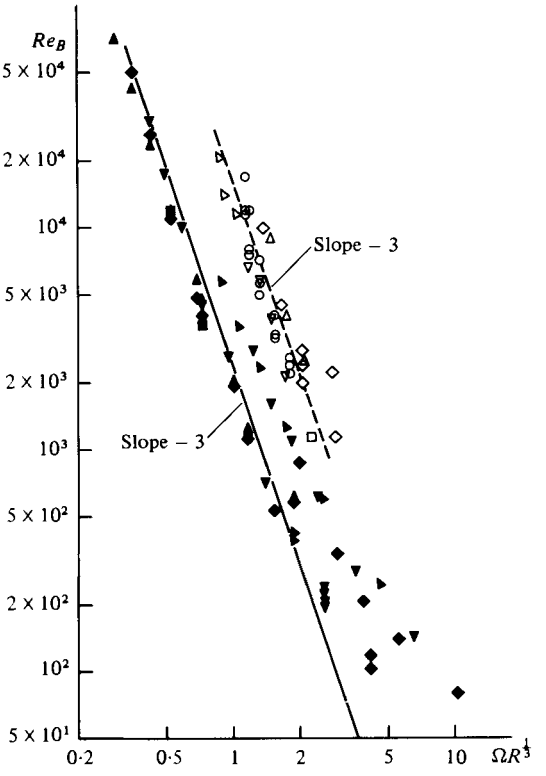

FIGURE 9. Vortex-breakdown data for flared vortex tubes and comparison with data of previous investigators. Present data, values of α: ▲, 3°; ◆, 10°; ■, 15°; ▼, 20°; ◢, 25°. Previous data: △, Sarpkaya (1971*a*); ○, Sarpkaya (1974); ◇, Ikeda *et al.* (1974); □, Bellamy-Knights (1976); ▽, Faler & Leibovich (1977); ◿, Garg & Leibovich (1979).

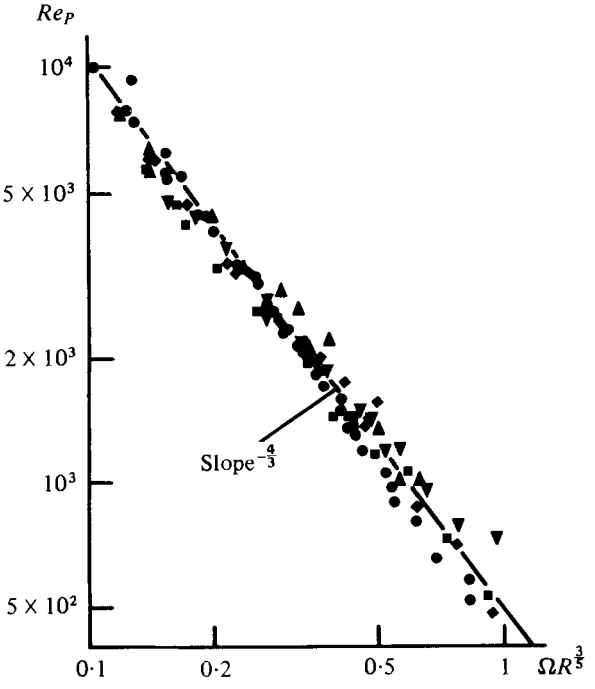

FIGURE 10. Pre-breakdown data for cylindrical contractions. For an explanation of the symbols see figure 5.

bulk of the data onto a single straight line with slope -3 is self evident, although there are significant departures for the narrowest slit, possibly because πDV is an overestimate for Γ in this case, a point which will be checked in a future series of measurements using the LDA system.

Breakdown data for flared contractions (with $R = 0{\cdot}012$ and $0{\cdot}046$) are plotted in figure 9 (together with data of previous investigators, to be discussed below) with the straight line from figure 8 included for reference. In general the trend is the same as for the cylindrical contractions, although breakdown occurs at measurably lower Reynolds numbers as α is increased. However, the differences may be regarded as small when it is considered that flare angles of up to 25° are included.

It is perhaps worthwhile to note that a better collapse of the vortex-breakdown data for both flared and cylindrical contractions is obtained if Re_B is plotted against $\Omega R^{\frac{1}{2}}$, although this appears to have no fundamental significance. The prebreakdown data of figure 5 may also be collapsed onto a single line, as shown in figure 10. However, the resulting form $Re_P \sim \Omega^{-\frac{4}{3}} R^{-\frac{4}{3}}$ is a purely empirical 'best fit' and should also be regarded as having no fundamental significance. The degree to which both the prebreakdown and breakdown data follow such simple trends is remarkable, especially considering that in the latter case many apparently different breakdown modes are included.

5. Discussion

Although previous investigators have generally given values for only Ω and Re_B for their experiments, from the details of their geometries it is a simple matter to evaluate the third parameter R. For reference, the ranges of values of Ω, R, Re_B and $\Omega R^{\frac{1}{2}}$ for a number of studies are listed in table 2.

Some care is necessary in interpreting the values given in this table. The Reynolds-number data, in particular, cover the entire range of conditions investigated in each case although in some instances experiments were limited to the occurrence of vortex breakdown, whereas in others disturbances at lower Reynolds numbers were also covered. Also, for experiments in flared tubes, both Ω and Re change somewhat with axial location, an influence which has not been included.

Two main factors complicate any attempt at comparisons of the work of different investigators. The first is the differences in geometries, especially regarding the turning section (figure 1). In particular, for all the guide-vane systems it is the case that $L/D \simeq 1$, which is precisely where our results show departures from the simple power-law relationship. The second factor is the probable influence of wall-friction effects in previous studies, as evidenced by the strong dependence of breakdown Reynolds number on axial location. The data in figure 9, extracted from the various investigations indicated, must be viewed with these cautionary remarks in mind. To make the comparison as fair as possible, only data for well-defined vortex breakdowns are included (spiral or bubble), and also only data for the furthest upstream locations where the wall-friction influence is the least significant (it will be recalled that our data were generally obtained at locations within one diameter of the contraction inlet) and for small flare angles. The data employed for the comparison are listed in table 3.

It seems reasonable to attribute to the difference in geometries the fact that the

Author(s)	Ω	R	$\Omega R^{\frac{1}{2}}$	Re
Sarpkaya (1971*a*)	1·2–3·0	0·35–0·88	1·15–2·11	$4{\cdot}6\times10^{2}$–$1{\cdot}1\times10^{4}$
Sarpkaya (1974)	0·8–2·4	0·43–1·34	0·88–1·81	6×10^{2}–$1{\cdot}8\times10^{4}$
Ikeda *et al.* (1974)	1·69–4·9	0·19–0·56	1·39–2·82	$1{\cdot}12\times10^{3}$–$1{\cdot}88\times10^{4}$
Bellamy-Knights (1976)	2·73	0·55	2·24	$1{\cdot}13\times10^{3}$
Faler & Leibovich (1977)	1·07–2·3	0·43–0·94	1·05–1·74	$8{\cdot}9\times10^{2}$–$6{\cdot}72\times10^{3}$
Garg & Leibovich (1979)	0·68–1·07	0·94–1·50	0·78–1·05	$1{\cdot}15\times10^{4}$–$2{\cdot}07\times10^{4}$
Present	0·66–46·4	0·012–0·058	0·26–10·5	$0{\cdot}80\times10^{2}$–$1{\cdot}04\times10^{5}$

TABLE 2. Parameter ranges for vortex-breakdown investigations.

Author(s)	Ω	$\Omega R^{\frac{1}{2}}$	R	$Re_B\times10^{-3}$
Sarpkaya (1971*a*)	1·75	1·48	0·60	9·0
	2·3	1·76	0·45	4·0
	3·0	2·11	0·35	2·5
Sarpkaya (1974)	1·2	1·15	0·88	17·0, 12·3, 11·6
	1·3	1·21	0·81	12·0, 8·0, 7·6
	1·5	1·33	0·70	7·2, 5·7, 5·0
	1·9	1·56	0·55	4·0, 3·3, 3·2
	2·4	1·81	0·43	2·6, 2·4, 2·2
Ikeda *et al.* (1974)	1·69	1·39	0·56	10·0
	2·24	1·66	0·41	4·5
	3·14	2·08	0·29	2·8, 2·0, 2·44
	4·89	2·81	0·19	2·24, 1·14
Bellamy-Knights (1976)	2·73	2·24	0·55	1·13
Faler & Leibovich (1977)	1·28	1·18	0·78	6·72
	1·54	1·33	0·65	5·83
	1·87	1·51	0·53	3·91
	2·30	1·74	0·43	2·13
Garg & Leibovich (1979)	1·07	1·05	0·94	11·5
	0·88	0·92	1·15	14·1
	0·82	0·88	1·14	20·7

TABLE 3. Vortex-breakdown data of previous investigators used for the purposes of comparison.

comparison data plotted in figure 9 lie considerably to the right of both the mean line for our cylindrical-tube data and also our data for flared contractions. The setups of Sarpkaya, Leibovich and his co-workers, and Ikeda *et al.* are practically identical in terms of the $\Omega \sim R$ relationship, and that of Bellamy-Knights is only slightly different. However, it is important to realize that the increase in L between the swirl vanes and the surface of diameter D_e (see L' in figure 1) results in an effective value of R which is considerably reduced owing to the fact that the fluxes of angular momentum and mass are conserved differently. Probably all that can be said with certainty is that these data do not contradict our contention that R is in general an independent parameter, and that for the geometries investigated to date the data are well represented by $Re_B \sim \Omega^{-3}R^{-1}$.

As noted earlier, we observe that in the case of the spiral form of vortex breakdown, the sense of the spiral is opposite to that of the outer flow, whereas for the prebreakdown disturbance the senses are the same. This change in character is a possible explanation for the discrepancy between our observations and those of previous investigators, with the exception of Lambourne & Bryer. An alternative explanation may lie in differences in the axial velocity distributions, which result from the different geometrical configurations. It may also be noted that, except at low Reynolds numbers, great care is necessary correctly to identify by eye the sense of the spiral.

7. Concluding remarks

Experimental evidence confirms dimensional arguments that to describe vortex breakdown and related flow phenomena, a parameter R representing the inflow angle is required in addition to the circulation number Ω and Reynolds number Re employed hitherto.

The new data presented here are well correlated by $Re_B \sim \Omega^{-3}R^{-1}$ over a wide range of Reynolds numbers (5×10^2–10^5) although departures are evident for very high circulation numbers and also for the lowest value of R ($= 0{\cdot}012$). This simple relationship is practically independent of both breakdown type and tube flare angle. The data of previous investigators follow a similar trend but with a significantly different constant of proportionality, attributed to differences in the experimental configurations involved. Although supported by theoretical arguments based upon the work of Benjamin (1962) and similarity concepts, it remains to be seen to what extent the above result is generally representative of vortex breakdown.

The experiments also show that vortex breakdown in a cylindrical tube is preceded, at a lower Reynolds number Re_P, by a prebreakdown disturbance. A purely empirical result which adequately correlates the data is $Re_P \sim \Omega^{-\frac{4}{5}}R^{-\frac{4}{5}}$. The sense of the prebreakdown disturbance is always the same as that of the outer flow, whereas for the spiral form of vortex breakdown the opposite holds true.

It is unfortunately the case that the experimental arrangement employed for the experiments described here is limited to small values of the parameter R. A new setup is under construction to permit coverage of a much wider range of values of R. Also planned are additional detailed measurements of the velocity fields for various vortex-flow regimes, especially in the vicinity of vortex breakdown. It is anticipated that these measurements will also throw further light on the possible connection between stability theory and vortex breakdown, first suggested by Garg & Leibovich (1979).

REFERENCES

Bellamy-Knights, P. G. 1976 A note on vortex breakdown in a cylindrical tube. *Trans. A.S.M.E.I., J. Fluids Engng* **98**, 322.

Benjamin, T. B. 1962 Theory of the vortex breakdown phenomenon. *J. Fluid Mech.* **14**, 593.

Cassidy, J. J. & Falvey, H. T. 1970 Observations of unsteady flow arising after vortex breakdown. *J. Fluid Mech.* **41**, 727.

Donaldson, C. du P. & Sullivan, R. 1960 Behaviour of solutions of the Navier–Stokes equations for a complete class of three-dimensional viscous vortices. *Proc. 1960 Heat Transfer Fluid Dyn. Inst.*, pp. 16–30. Stanford University Press.

ESCUDIER, M. P., BORNSTEIN, J. & ZEHNDER, N. 1980*a* Observations and LDA measurements of confined turbulent vortex flow. *J. Fluid Mech.* **98**, 49.

ESCUDIER, M. P., BORNSTEIN, J., ZEHNDER, N. & MAXWORTHY, T. 1980*b* Classification of confined-vortex flow regimes. In *Vortex Flows* (ed. W. L. Swift & P. S. Barna). A.S.M.E.

FALER, J. H. & LEIBOVICH, S. 1977 Disrupted states of vortex flow and vortex breakdown. *Phys. Fluids* **20**, 1385.

FALER, J. H. & LEIBOVICH, S. 1978 An experimental map of the internal structure of a vortex breakdown. *J. Fluid Mech.* **86**, 313.

GARG, A. K. & LEIBOVICH, S. 1979 Spectral characteristics of vortex breakdown flow fields. *Phys. Fluids* **22**, 2053.

HARVEY, J. K. 1962 Some observations of the vortex breakdown phenomenon. *J. Fluid Mech.* **14**, 585.

IKEDA, T., SAKATA, M. & KIKUCHI, K. 1974 An experimental study on vortex breakdown in straight and divergent pipes. *J. Fac. Engng, Shishu Univ., Japan* **36**, 1.

KIRKPATRICK, D. L. I. 1964 Experimental investigation of the breakdown of a vortex in a tube. *Aero. Res. Counc. Current Paper*, no. 821.

LAMBOURNE, N. C. 1965 The breakdown of certain types of vortex. *Aero. Res. Counc. Current Paper*, no. 915.

LAMBOURNE, N. C. & BRYER, D. W. 1961 The bursting of leading-edge vortices – Some observations and discussion of the phenomenon. *Aero. Res. Counc. R. & M.*, no. 3282.

SARPKAYA, T. 1971*a* On stationary and travelling vortex breakdowns. *J. Fluid Mech.* **45**, 545.

SARPKAYA, T. 1971*b* Vortex breakdown in swirling conical flows. *A.I.A.A.J.* **9**, 1972.

SARPKAYA, T. 1974 Effect of the adverse pressure gradient on vortex breakdown. *A.I.A.A.J.* **12**, 602.

TITCHENER, I. M. & TAYLOR-RUSSELL, A. J. 1956 Experiments on the growth of vortices in turbulent flow. *Aero. Res. Counc. Current Paper*, no. 316.